Phys. Lett. B 869 (2025) 139839

Contents lists available at ScienceDirect

Physics Letters B

journal homepage: www.elsevier.com/locate/physletb

Letter

Lattice simulation of nucleon distribution and shell closure in the proton-rich nucleus ^{22}Si

Shuang Zhang [a], Serdar Elhatisari [b,c], Ulf-G. Meißner [a,d,e,*], Shihang Shen [a,e]

[a] Institute for Advanced Simulation (IAS-4) Forschungszentrum Jülich, D-52425, Jülich, Germany
[b] King Fahd, University of Petroleum and Minerals (KFUPM), 31261, Dhahran, Saudi Arabia
[c] Faculty of Natural Sciences and Engineering, Gaziantep Islam Science and Technology University, 27010, Gaziantep, Turkey
[d] Bethe Center for Theoretical Physics and Helmholtz-Institut für Strahlen- und Kernphysik, Universität Bonn, D-53115, Bonn, Germany
[e] Peng Huanwu Collaborative Center for Research and Education, International Institute for Interdisciplinary and Frontiers, Beihang University, 100191, Beijing, China

ARTICLE INFO

Editor: Dr A Schwenk

Keywords:
Effective field theory
Lattice
Silicon
Shell closure

ABSTRACT

The proton-rich nucleus ^{22}Si is studied using Nuclear Lattice Effective Field Theory with high-fidelity chiral forces. Our results indicate that ^{22}Si is more tightly bound than ^{20}Mg, thereby excluding the possibility of two-proton emission. The $Z = 14$ shell closure in ^{22}Si is investigated through the evolution of the 2^+ state in the neighboring nuclei. We then focus on the charge radius and spatial distribution information of ^{22}Si, considering the novel phenomena that may emerge due to the small two-proton separation energy and the shell closure. We present the distribution of the 14 protons and 8 neutrons obtained from our lattice simulation, revealing insights into the spatial arrangement of the nucleons. Moreover, the spatial localization of the outermost proton and neutron suggests that ^{22}Si is a doubly magic nucleus. Furthermore, we develop the pinhole method based on the harmonic oscillator basis, which gives insight into the nuclear structure in terms of the shell model picture from lattice simulations. Our calculated occupation numbers support that $Z = 14$ and $N = 8$ are the shell closures and show that the $\pi 1s_{1/2}$ orbital component is minor in ^{22}Si.

1. Introduction

Nuclei exhibiting a significant neutron-proton imbalance reveal novel insights into nuclear structure and nuclear astrophysics, but they pose major challenges to theoretical approaches. Recent discoveries of a growing number of proton-rich nuclei have significantly impacted our understanding of nuclear symmetries [1–3], shell evolution [4,5], astrophysical processes [6], and proton emission [7,8]. Notably, the locations of the proton dripline for the P, S, and Ar elements have been accurately determined [9]. Moving further down the nuclear chart, the nucleus ^{22}Si emerges as a particularly intriguing case due to its proximity to the proton dripline and its unique occupancy of the $Z = 14$ subshell and $N = 8$ shell. It is probably the lightest bound nucleus with the $T_Z = -3$, where T denotes the nuclear isospin. Nuclei located at shell closures are key to understanding nuclear structure, and the evolution of nuclear structure in exotic nuclei, influenced by nuclear forces and many-body correlations, is also of significant interest. Hence, we focus on ^{22}Si as the first test case for Nuclear Lattice Effective Field Theory (NLEFT) [10] calculations of the proton-rich region, which can probe the isospin symmetries and the evolution of certain properties in exotic regions of the nuclear chart, and provide essential tests to the nuclear forces and many-body correlations.

Much remains to be explored regarding the properties of ^{22}Si, both from experimental and theoretical perspectives. It was initially observed at GANIL [11], and its spectrum was subsequently studied [12]. Recent experiments have indirectly measured its ground-state (g.s.) mass [13,14], but inconsistencies in the resulting two-proton emission properties necessitate further direct experimental measurements and theoretical studies. From the theoretical side, *ab initio* calculations also suggest varying predictions for the two-proton separation energy [15–17]. Moreover, the large proton-neutron asymmetry ($|N - Z| = 6$) in ^{22}Si suggests that its charge radius could provide new constraints on the slope L of the symmetry energy in the equation of state [18,19] when combined with data for its mirror partner ^{22}O. In addition, the isospin asymmetry observed in the ^{22}Si/^{22}O Gamow-Teller transition [20] and the first mass measurement of ^{22}Al [21,22], respectively, revealed and suggested the halo structure in ^{22}Al. Given that ^{22}Si lies nearer the edge of the nuclear landscape, it is fascinating to explore how its shell closure and proton-neutron imbalance compete, and to investigate the $\pi 1s_{1/2}$ component in ^{22}Si, which also gained a lot of attention

* Corresponding author.
E-mail address: meissner@hiskp.uni-bonn.de (U. Meißner).

https://doi.org/10.1016/j.physletb.2025.139839
Received 25 May 2025; Received in revised form 17 July 2025; Accepted 20 August 2025
Available online 22 August 2025

in studies of the bubble nuclei ^{34}Si on the neutron-rich side of silicon isotopes [23].

In this work, we perform Monte Carlo simulations for ^{22}Si in the framework of NLEFT with high-fidelity nucleon-nucleon (NN) and three-nucleon (3N) forces at next-to-next-to-next-to-leading order (N^{3}LO) [24]. Using the pinhole algorithm [25] and the newly proposed pinhole algorithm based on the harmonic oscillator (HO) basis, we are able to probe the inner structure of ^{22}Si. With these theoretical methods, we compute the binding energies and first 2^+ states of ^{22}Si and its neighboring nuclei using a global chiral NN and 3N interaction [24], as well as an interaction specifically fine-tuned for silicon isotopes [19]. We suggest that ^{22}Si is a dripline nucleus and discuss the $Z = 14$ shell closure using the evolution of the 2^+ states in $N = 8$ isotones. We also give predictions for the radii of ^{22}Si, and show the charge radius difference (CRD) with its mirror partner ^{22}O. Finally, we focus on the nucleon distributions of ^{22}Si and present the occupation numbers for the g.s. of ^{22}Si. Very recently, new experimental data on ^{22}Si have been reported in Ref. [26], providing direct measurements of its mass and insights into its shell closure. These results serve as valuable benchmarks and offer strong validation of the predictions presented in this work.

2. Methods

NLEFT has the advantage of capturing the full set of many-body correlations with the use of auxiliary-field Monte Carlo simulations, but suffers from severe sign problems in its application to high-fidelity chiral forces described by the chiral Hamiltonian H_χ. In Ref. [24], the wavefunction matching method was developed which maps the unitarily transformed $H'_\chi = U H_\chi U$ to a simple Hamiltonian H_S, where the H_S is largely free of sign oscillations. This simple Hamiltonian consists of smeared two-nucleon contact interactions as well as regularized one-pion exchange. If H'_χ is sufficiently close to H_S, first-order perturbation theory can be used efficiently to calculate the higher-order chiral forces up-to-and-including N^{3}LO. Furthermore, smeared 3NFs are then fitted to masses of selected nuclei ranging from $A = 3$ to $A = 40$. Consequently, nuclear charge radii as well the equation of state for neutron and for nuclear matter can be predicted, showing good agreement with the data. We use the same Hamiltonian in this study and refer to Ref. [24] for further details. To further study the systematic uncertainties of our calculations, we also use the modified version of the 3NFs that was fine-tuned to the binding energies of the silicon isotopic chain [19], and we refer to the chiral force from Ref. [24] as global interaction in what follows.

In this work, we perform simulations on a periodic cubic lattice with a side length of $L = 10$ and lattice spacing $a \simeq 1.32$ fm, corresponding to a momentum cutoff $\Lambda = \pi/a \simeq 471$ MeV and to a physical length $L \times a = 13.2$ fm. In our calculations, the Euclidean time evolution of the initial states is discretized into L_t steps, separated by a temporal lattice spacing a_t, such that the Euclidean time is $\tau = L_t \times a_t$. Consequently, the time-evolution operator is represented as a series of L_t transfer matrices, $M^{L_t} = \left[: \exp(-H_S a_t) : \right]^{L_t}$, using the Trotter decomposition where the :: symbol indicates normal ordering. The temporal lattice spacing is set to $a_t = 0.001$ MeV^{-1}. In the Euclidean time evolution, the initial states are chosen as products of single-particle harmonic oscillator wave functions. Subsequently, the chiral Hamiltonian H'_χ is calculated perturbatively [27] using the wave functions evolved in Euclidean time. All the calculated energies and radii are extrapolated to the infinite Euclidean time limit using the formalism from Refs. [28–30], while the nucleon distribution and occupation number simulations are performed at $\tau = 0.2$ MeV^{-1} (as discussed in [31]). We note that the statistical uncertainties on the one hand stem from the Monte Carlo simulations and on the other hand from the Euclidean time extrapolation. The systematic error are obtained by considering two different sets of interaction parameters. More details on the uncertainty quantification can be found in Ref. [24].

For the radii and nucleon distribution calculations, we employ the pinhole algorithm [25], details are presented in [31]. To gain more insight into the nuclear structure, we propose here a variation of the pinhole method based on the HO basis to estimate the occupation numbers of shell model orbitals. With this approach, we aim to establish a bridge between the Monte Carlo simulations in coordinate or momentum space and the shell model in configuration space. Instead of sampling the nucleon positions and spin-isospin as proposed in the standard pinhole algorithm, we sample the HO basis characterized by the principal, orbital angular momentum, total angular momentum, and angular momentum projection quantum number. Further details can be found in [31].

3. Results

In Fig. 1, we present the calculated g.s. energies of ^{22}Si and ^{20}Mg with different τ and extrapolate to infinite Euclidean time. We get $-133.66(28)$ MeV and $-134.38(39)$ MeV for ^{20}Mg and ^{22}Si, respectively, whereas experiment gives -134.56 MeV for ^{20}Mg [32]. For ^{22}Si, there is no direct experimental measurement, however, the indirect measurement gives -134.45 MeV [13]. The β-delayed one-proton and two-proton emissions in ^{22}Si have been measured, while two-proton decay has not yet been ruled out [13,14]. *Ab initio* calculations based on chiral forces yield varying predictions for the two-proton separation energies of ^{22}Si [15–17]. Our calculations indicate that ^{22}Si is more bound than ^{20}Mg within the statistical error. Specifically, when the maximum τ is increased from 0.3 MeV^{-1} to 0.4 MeV^{-1}, the extrapolated g.s. energies for both nuclei change by less than 0.36 MeV, and ^{22}Si consistently remains more bound than ^{20}Mg. It yields a two-proton separation energy of $S_{2p} = 0.72(48)$ MeV with maximum $\tau = 0.4$ MeV^{-1}, which suggests that ^{22}Si is not a $2p$ emission candidate. Furthermore, we also employed an alternative set of chiral forces proposed for silicon isotopes for a sensitivity analysis [19]. The calculated g.s. energies of ^{22}Si and ^{20}Mg are $-136.28(41)$ MeV and $-134.94(18)$ MeV, respectively. The extracted S_{2p} is 1.34(45) MeV, which is consistent with the prediction from the global

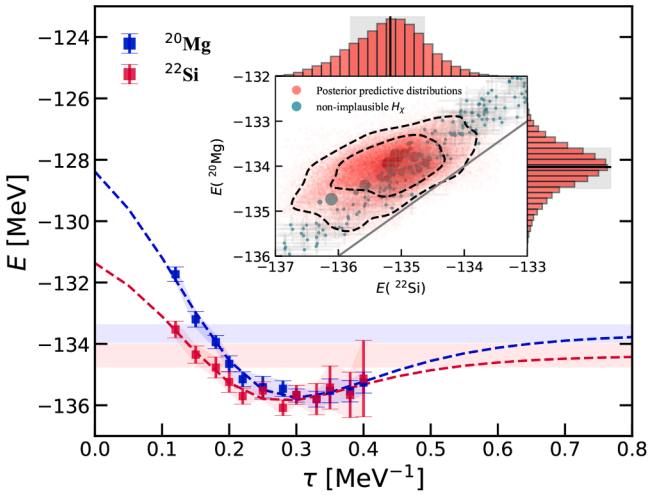

Fig. 1. Calculated g.s. energies of ^{22}Si and ^{20}Mg using the global interaction. Red and blue squares represent the results for ^{22}Si and ^{20}Mg as functions of Euclidean time, with error bars and shaded regions indicating statistical uncertainties. Dashed lines represent extrapolated curves with error bands centered on the extrapolated energies. **Inset:** The teal circles represent the g.s. energies of ^{22}Si and ^{20}Mg from non-implausible prior samples obtained via history matching [24], including uncertainties. Posterior samples are shown as red points, with dashed lines indicating the 1σ and 2σ credible intervals. The solid grey line indicates the condition $E(^{22}\mathrm{Si}) = E(^{20}\mathrm{Mg})$. Marginal histograms are shown on each axis along with the statistical median and 1σ credible intervals. (For interpretation of the references to colour in this figure legend, the reader is referred to the web version of this article.)

interaction. To further quantify the impact of the chiral force uncertainties on the predictions, we performed a Bayesian analysis with a set of non-implausible samples [24] obtained via history matching [33–35]. The results are shown in the inset of Fig. 1. Based on the Bayesian posterior distributions constrained by the g.s. energies of ^{18}Ne and ^{20}Mg, the estimated median and 1σ credible intervals for the g.s. energy and S_{2p} of ^{22}Si are $-135.14^{+0.60}_{-0.60}$ MeV and $1.05^{+0.53}_{-0.49}$ MeV, respectively. Furthermore, S_{2p} remains positive within the 2σ interval, indicating with 95 % credibility that ^{22}Si is bound than ^{20}Mg.

We then focus on the evolution of 2^+ states in ^{22}Si and its nearby $N = 8$ isotones as a key indicator of the $Z = 14$ shell closure. In Fig. 2, we show the calculated 2^+ states of ^{18}Ne, ^{20}Mg and ^{22}Si with two sets of chiral forces, and compare with experiment [36]. The energies of the 2^+ states in ^{18}Ne, ^{20}Mg, and ^{22}Si based on the global interaction are 1.70(44) MeV, 1.47(32) MeV, and 2.11(57) MeV, respectively, while the results based on the alternative interaction are 1.69(51) MeV, 1.38(40) MeV, and 1.98(70) MeV, respectively. The energies of 2^+ states extracted from these two calculations are in good agreement. While a measurement for 2^+ state in ^{22}Si is not yet available, the calculated 2^+ states of ^{18}Ne and ^{20}Mg agree with the experimental values of 1.89 MeV and 1.60 MeV. The calculated central value of the 2^+ excitation energy in ^{22}Si are higher than those of the other $N = 8$ isotones, suggesting a possible $Z = 14$ subshell closure at the proton dripline. However, due to the large statistical uncertainties in the calculations, this remains a tentative indication requiring further confirmation. Since $N = 8$ is a conventional magic number, proton excitation may challenge the notion of estimating the neutron shell structure in $Z = 14$ isotopes through the energies of the 2^+ state [37]. We will later use the pinhole method to calculate the nucleon distributions and occupation numbers on the HO basis. Meanwhile, these results provide valuable insights into the characteristics of the $N = 8$ shell.

Next, we use the pinhole method to calculate the charge radius of the ^{22}Si g.s. and its radius difference with neighboring nuclei [31]. In Table 1, we present the calculated charge radii $R_{\rm ch}$ for the ^{22}Si g.s. from the global interaction and the chiral forces fine-tuned for the silicon isotopes [19]. While the results are generally consistent, subtle differences highlight systematic uncertainties in the nuclear interactions. Additional sources of systematic uncertainty, such as spin-orbit corrections to the charge radius [38–40] and finite-volume effects, all of which require more detailed exploration in future work. At present, we combine these results to estimate the radius at the 3σ confidence level, yielding a range from 3.145 to 3.334 fm. The calculated radii of ^{20}Mg with these interactions are 3.207(24) fm, and 3.126(22) fm, respectively. We find the $\Delta R_{\rm ch}$ between ^{22}Si and ^{20}Mg obtained by two sets of chiral forces are consistent. The extracted $\Delta R_{\rm ch}$ between ^{22}Si and ^{20}Mg is 0.070 fm, which is comparable to the $\Delta R_{\rm ch}(^{28}\text{Si-}^{26}\text{Mg}) = 0.088$ fm, $\Delta R_{\rm ch}(^{30}\text{Si-}^{28}\text{Mg}) = 0.064$ fm and $\Delta R_{\rm ch}(^{32}\text{Si-}^{30}\text{Mg}) = 0.042$ fm measured in experiments [19,41]. The $\Delta R_{\rm ch}$ between these isotopes of silicon and magnesium is of a similar magnitude, indicating similar underlying nuclear structure effects may influence the charge distribution in the dripline nucleus ^{22}Si, despite its relatively small S_{2p}. In addition, we calculated the mirror CRD for the ^{22}Si – ^{22}O mirror pair. The correlation between the mirror CRD and the slope L in the symmetry energy was found to be $\Delta R_{\rm ch} \propto |N - Z| \times L$ in the density function theory calculation [42], and has been used to constrain the L [18,43]. With a large proton-neutron imbalance $|N - Z| = 6$, the $\Delta R_{\rm ch}$ between the ^{22}Si – ^{22}O mirror pair will significantly constrain L. However, recent studies suggest that pairing correlations induced by the proton continuum [44,45], and quantum many-body effects [35] may influence the constraint relations in the ^{36}Ca – ^{36}S mirror pair. The interplay between nuclear spatial extension, many-body correlations, and weak binding makes ^{22}Si a valuable candidate for providing insights into many-body correlations, nuclear forces, or constraints on the symmetry energy slope. Incorporating full many-body correlations, our calculated mirror charge radii between the ^{22}Si – ^{22}O mirror pair with chiral NN + 3N forces show good agreement. In Ref. [46], a linear relationship between the mirror CRD and isospin difference was established, predicting $\Delta R_{\rm ch} = 0.429(21)$ fm for the ^{22}Si – ^{22}O mirror pair. Our lattice simulation results are relatively small but remain consistent with this prediction within the 3σ confidence level. Here we also give the slope $L = 56.4(5.8)$ MeV extracted based on the global interaction [24] for reference. In the following, we will focus on the spatial distribution of ^{22}Si and discuss the impact of higher HO orbitals close to the particle continuum on ^{22}Si.

Table 1
Charge radii ($R_{\rm ch}$), CRD $\Delta R_{\rm ch}(^{22}\text{Si-}^{20}\text{Mg}) = R_{\rm ch}(^{22}\text{Si}) - R_{\rm ch}(^{20}\text{Mg})$ and mirror CRD $\Delta R_{\rm ch}(^{22}\text{Si-}^{22}\text{O}) = R_{\rm ch}(^{22}\text{Si}) - R_{\rm ch}(^{22}\text{O})$ of ^{22}Si calculated with the global chiral forces [24] and chiral forces fine-tuned for the silicon isotopes [19]. All values are given in fm and include statistical errors.

	$R_{\rm ch}$	$\Delta R_{\rm ch}(^{22}\text{Si-}^{20}\text{Mg})$	$\Delta R_{\rm ch}(^{22}\text{Si-}^{22}\text{O})$
H_χ [24]	3.277 (19)	0.070 (31)	0.361 (32)
H_χ [19]	3.196 (17)	0.070 (28)	0.370 (29)

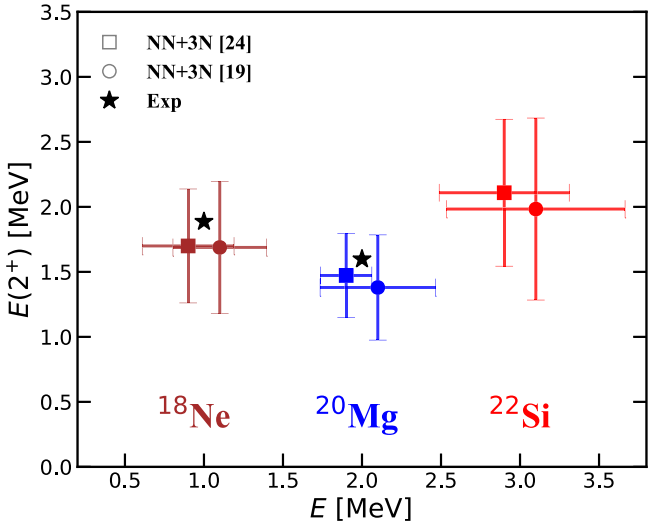

Fig. 2. Excitation energies of $J = 2^+$ states in the $N = 8$ isotones ^{18}Ne, ^{20}Mg and ^{22}Si (experiment [36]: black stars, theory: squares and circles). Squares show results from the global interaction, while circles represent results from interaction for silicon isotopes. Vertical solid lines indicate uncertainties in the excitation energies, while horizontal solid lines show uncertainties in the absolute energies of 2^+ states due to Euclidean time extrapolation. The horizontal position of the symbols along the E-axis serves only to visually separate different isotones and carries no physical meaning. The axis scale reflects only the uncertainty in the absolute energy extrapolation of the 2^+ states.

We use the pinhole method [25] to simulate the position distribution of A nucleons. As described in Ref. [25], the point-nucleon positions are convolved with a Gaussian distribution to account for the finite size of the nucleons. To enhance the smoothness and reduce lattice artifacts in the density profiles, we apply 1000 additional iterations of Gaussian smearing for each pinhole configuration. In each simulation, the nucleon coordinates are rearranged from small to large based on the distance of each nucleon relative to the center-of-mass (CoM). It is important to emphasize that this ordering does not correspond to labeling individual nucleons, but serves as a statistical characterization of the spatial information across the entire ensemble of simulated configurations. This enables us to gain meaningful information about the spatial structure, such as the maximum spatial extent of the nucleons as indicated by the outermost nucleon distribution. In Fig. 3, we show the simulated proton distributions in ^{22}Si and ^{20}Mg based on the global interaction. Due to the sign problem, the nucleon distributions sometimes become

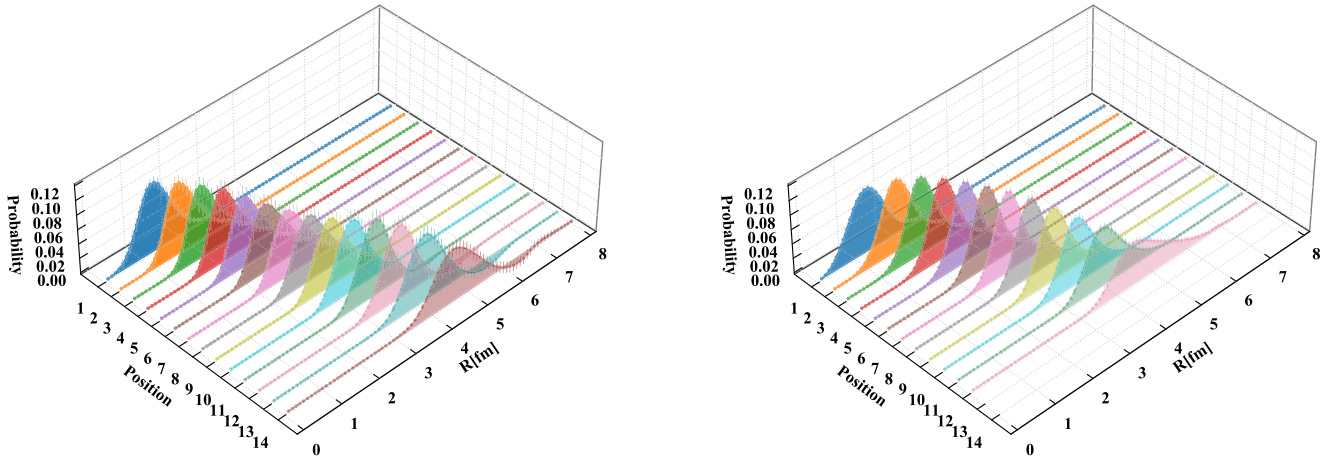

Fig. 3. Proton distribution probabilities in ^{22}Si (left panel) and ^{20}Mg (right panel) simulated using the pinhole method with the global chiral force at N^{3}LO. The colors represent the distribution of Z groups of protons, ranging from near to far relative to the CoM. The uncertainty in the simulation is represented by the error bar.

negative, however, within the bounds of the statistical uncertainty, and these values are very close to zero.

We find that the outermost proton distribution in ^{20}Mg is more extended than the other proton distributions. As shown in [31], we also observe this phenomenon in the outermost neutron distribution of ^{5}He and ^{6}He. The degree of nucleon binding is reflected in the extension of the outermost nucleon distribution. In the simulation of ^{22}Si using the high-fidelity forces, we observe that the outermost proton distribution is similar to that of the inner layers, resulting in a less extended spatial distribution compared to that observed in ^{20}Mg. Moreover, the outermost neutron distribution in ^{22}Si exhibits spatial localization characteristics and shows a similar broadening pattern to those of the inner nucleon distributions, as also shown in [31]. These spatial localizations reveal, to a certain extent, the presence of shell closure at $Z = 14$ and $N = 8$ in ^{22}Si, indicating that ^{22}Si is a doubly magic nucleus at the proton dripline. Additionally, we find in our calculations that the general features of the chiral force significantly enhance the $Z = 14$ shell closure compared to the simple Hamiltonian. As detailed in [31], we perform an in-depth analysis of each set of proton distributions by calculating the average distances derived from these distributions. This study reveals the structural similarity between the proton distributions of $N = 8$ isotones ^{22}Si and ^{20}Mg, explores the preferred spatial positions of the two extra protons in ^{22}Si, and demonstrates that the outmost proton in ^{22}Si is more tightly packed in space.

Using the pinhole method within the HO basis, we calculated the HO orbitals occupation numbers of ^{22}Si with the empirical parameter $\hbar\omega = 41A^{-1/3}$ MeV and global interaction. These calculations provide a detailed insight into the nucleon distributions across the HO orbitals, revealing the underlying shell structure of ^{22}Si. In [31], we present several HO orbital occupation numbers of neutrons (n_ν) and protons (n_π) in ^{22}Si. For the neutron occupation numbers, it is evident that the $N = 8$ shell is fully occupied, indicating a minimal contribution from higher HO orbitals and confirming the presence of the $N = 8$ shell closure. Regarding the proton occupation numbers, the $Z = 14$ shell is also nearly fully occupied. The $0d_{5/2}$ orbitals are predominantly occupied, though with relatively larger statistical errors compared to the occupations of the inner shell. These results further support our conclusions regarding the existence of $Z = 14$ and $N = 8$ shell closures from the spatial distribution of nucleons. Furthermore, the low occupancy of the $1s_{1/2}$ orbital reflects a minor proton $1s$ wavefunction component on the proton-rich side of the silicon isotopes. This also indicates the closed-shell effect in ^{22}Si remains dominant, outweighing the impact of the proton-neutron imbalance at the landscape boundary.

4. Conclusions

We have used NLEFT to understand the structure of the ^{22}Si nucleus. Using two sets of chiral NN and 3N forces at N^{3}LO, we calculated the binding energies and 2^+ excitation energies of ^{22}Si, ^{20}Mg, and ^{18}Ne. Overall results are in agreement with the available experimental data and predict that ^{22}Si is a dripline nucleus, as well as the possible presence of a shell closure at $Z = 14$ in ^{22}Si. Additionally, we calculated the charge radius of ^{22}Si, and extracted the mirror charge radius difference, which can serve as a reference for future experiments. Finally, insights into the ^{22}Si structure have been demonstrated in both coordinate and configuration space using the pinhole method. We simulated the spatial distribution characteristics of nucleons and extracted the HO basis occupation numbers in ^{22}Si. It further supports the ^{22}Si is a doubly magic nucleus and unveils detailed nucleon information within the nucleus while accounting for the full set of many-body correlations. While the work presented here offers a new perspective on exploring nuclear structure, many other ways remain to be explored for a more comprehensive understanding.

Data availability

No data was used for the research described in the article.

Declaration of competing interest

The authors declare that they have no known competing financial interests or personal relationships that could have appeared to influence the work reported in this paper.

Acknowledgements

We are grateful for discussions with Dean Lee and other members of the NLEFT collaboration. This work is part of the EXOTIC grant and was supported in part by the European Research Council (ERC) under the European Union's Horizon 2020 research and innovation programme (grant agreement No. 101018170). The work of UGM was also supported by the CAS President's International Fellowship Initiative (PIFI) (Grant No. 2025PD0022). The work of SE is supported in part by the Scientific and Technological Research Council of Turkey (TUBITAK project no. 123F464). The authors gratefully acknowledge the Gauss Centre for Supercomputing e.V. (https://www.gauss-centre.eu) for funding this project by providing computing time on the GCS Supercomputer JUWELS at Jülich Supercomputing Centre (JSC).

Supplementary material

Supplementary material associated with this article can be found in the online version at 10.1016/j.physletb.2025.139839

References

[1] T.B. Webb, et al., Phys. Rev. Lett. 122 (2019) 122501, arXiv preprint arXiv: 1812.08880 [nucl-ex]
[2] L. Lalanne, et al., Phys. Rev. Lett. 129 (2022)122501, arXiv preprint arXiv: 2201.01513 [nucl-ex]
[3] J. J. Liu et al. (RIBLL), Phys. Rev. Lett. **129**, 242502 (2022)
[4] L. Lalanne et al., Phys. Rev. Lett. **131**, 092501 (2023), arXiv preprint arXiv: 2302.14382 [nucl-ex]
[5] Y. Jin et al., Phys. Rev. Lett. **127**, 262502 (2021)
[6] A. M. Rogers et al., Phys. Rev. Lett. **106**, 252503 (2011)
[7] R. J. Charity et al., Phys. Rev. Lett. **131**, 172501 (2023)
[8] M. Pfützner, I. Mukha, S. Wang, Prog. Part. Nucl. Phys. **132**, 104050 (2023), arXiv preprint arXiv: 2304.13391 [nucl-ex]
[9] Y. Yu et al., Phys. Rev. Lett. **133**, 222501 (2024), arXiv preprint arXiv: 2410.17701 [nucl-ex]
[10] T. A. Lähde and U.-G. Meißner, *Nuclear Lattice Effective Field Theory: An Introduction*, Vol. 957 (Springer, 2019)
[11] M. G. Saint Laurent et al., Phys. Rev. Lett. **59**, 33 (1987)
[12] B. Blank et al., Phys. Rev. C **54**, 572 (1996)
[13] X. X. Xu et al., Phys. Lett. B **766**, 312 (2017)
[14] M. Babo, *β-Delayed Charged Particle Decays of Neutron-Deficient Nuclei* ^{20}*Mg and* ^{22,23}*Si*, Theses, Université de Caen Normandie (2016)
[15] J.D. Holt, J. Menendez, A. Schwenk, Phys. Rev. Lett. **110**, 022502 (2013), arXiv preprint arXiv: 1207.1509 [nucl-th]
[16] S.R. Stroberg, J.D. Holt, A. Schwenk, and J. Simonis, Phys. Rev. Lett. **126**, 022501 (2021), arXiv preprint arXiv: 1905.10475 [nucl-th]
[17] S. Zhang, Y.Z. Ma, J.G. Li, B.S. Hu, Q. Yuan, Z.H. Cheng, and F.R. Xu, Phys. Lett. B **827**, 136958 (2022), arXiv preprint arXiv: 2112.02844 [nucl-th]
[18] S.V. Pineda et al., Phys. Rev. Lett. **127**, 182503 (2021), arXiv preprint arXiv: 2106.10378 [nucl-th]
[19] K. König et al., Phys. Rev. Lett. **132**, 162502 (2024), [Erratum: Phys. Rev .Lett. 133, 059901 (2024)], arXiv preprint arXiv: 2309.02037 [nucl-th]
[20] J. Lee et al., Phys. Rev. Lett. **125**, 192503 (2020)
[21] M.Z. Sun et al., Chin. Phys. C **48**, 034002 (2024), arXiv preprint arXiv: 2401.14704 [nucl-th]
[22] S.E. Campbell et al., Phys. Rev. Lett. **132**, 152501 (2024), arXiv preprint arXiv: 2312.11366 [nucl-th]
[23] A. Mutschler et al., Nature Phys. **13**, 152 (2017), arXiv preprint arXiv: 1707.03583 [nucl-th]
[24] S. Elhatisari et al., Nature **630**, 59 (2024), arXiv preprint arXiv: 2210.17488 [nucl-th]
[25] S. Elhatisari et al., Phys. Rev. Lett. **119**, 222505 (2017), arXiv preprint arXiv: 1702.05177 [nucl-th]
[26] Y.M. Xing et al., Phys. Rev. Lett. **135**, 012501 (2025), arXiv preprint arXiv: 2503.01380 [nucl-th]
[27] B.N. Lu, N. Li, S. Elhatisari, D. Lee, E. Epelbaum, U.-G. Meißner, Phys. Lett. B **797**, 134863 (2019), arXiv preprint arXiv: 1812.10928 [nucl-th]
[28] T.A. Lähde, E. Epelbaum, H. Krebs, D. Lee, U.-G. Meißner, G. Rupak, J. Phys. G **42**, 034012 (2015), arXiv preprint arXiv: 1409.7538 [nucl-th]
[29] R. He, N. Li, B.N. Lu, D. Lee, Phys. Rev. A **101**, 063615 (2020), arXiv preprint arXiv: 1910.01257 [nucl-th]
[30] S. Shen, S. Elhatisari, T.A. Lähde, D. Lee, B.N. Lu, U.-G. Meißner, Nature Commun. **14**, 2777 (2023), arXiv preprint arXiv: 2202.13596 [nucl-th]
[31] See Supplemental Material for the discussion of the pinhole algorithm in coordinate and HO space, the occupation number calculations, the charge radius calculations, the distribution of neutrons and the average proton distribution distances in various nuclei.
[32] A.T. Gallant et al., Phys. Rev. Lett. **113**, 082501 (2014), arXiv preprint arXiv: 1409.1477 [nucl-th]
[33] I. Vernon, J. Liu, M. Goldstein, J. Rowe, J. Topping, and K. Lindsey, BMC Systems Biology **12**, 1 (2018)
[34] B.S. Hu et al., Nature Phys. **18**, 1196 (2022), arXiv preprint arXiv: 2112.01125 [nucl-th]
[35] B.S. Hu, Phys. Lett. B **857**, 138969 (2024), arXiv preprint arXiv: 2408.17403 [nucl-th]
[36] https://www.nndc.bnl.gov/ensdf/
[37] J.G. Li, H.H. Li, S. Zhang, Y.M. Xing, and W. Zuo, Phys. Lett. B **846**, 138197 (2023)
[38] A. Ong, J.C. Berengut, V.V. Flambaum, Phys. Rev. C **82**, 014320 (2010), arXiv preprint arXiv: 1006.5508 [nucl-th]
[39] C.J. Horowitz, J. Piekarewicz, Phys. Rev. C **86**, 045503 (2012), arXiv preprint arXiv: 1208.2249 [nucl-th]
[40] G. Hagen et al., Nature Phys. **12**, 186 (2015), arXiv preprint arXiv: 1509.07169 [nucl-th]
[41] D.T. Yordanov et al., Phys. Rev. Lett. **108**, 042504 (2012)
[42] B.A. Brown, Phys. Rev. Lett. **119**, 122502 (2017)
[43] B.A. Brown et al., Phys. Rev. Res. **2**, 022035 (2020)
[44] A.J. Miller et al., Nature Phys. **15**, 432 (2019)
[45] P.-G. Reinhard and W. Nazarewicz, Phys. Rev. C **105**, L021301 (2022), arXiv preprint arXiv: 2201.02238 [nucl-th]
[46] S.J. Novario, D. Lonardoni, S. Gandolfi, G. Hagen, Phys. Rev. Lett. **130**, 032501 (2023), arXiv preprint arXiv: 2111.12775 [nucl-th]